**Appendix**

**The following pages numbered 400-403 is a copy of the publication:**

- Brian Julsgaard, Alexander Kozhekin & Eugene S. Polzik, "Experimental long-lïved entanglement of two macroscopic objects", NATURE, VOL 413, 27 SEPTEMBER 2001, pages 400-403.

It is referred as [D1].

16. Lee, P. C. *Physical Properties and Processing of Asteroid Regoliths and Interiors*. Thesis, Cornell Univ. (1997).
17. Thomas, P. C., Veverka, J., Robinson, M. S. & Murchie, S. Shoemaker crater as the source of most ejecta blocks on the asteroid 433 Eros. *Nature* 413, 394–396 (2001).
18. Cotswell, D. R. in *Photon and Particle Interactions with Surfaces in Space* (ed. Grard, R. J. L.) 543–556 (Reidel, Dordrecht, 1973).

**Acknowledgements**

We thank the mission design, mission operations, and spacecraft teams of the NEAR Project at the Applied Physics Laboratory of Johns Hopkins University and the navigation team at the Jet Propulsion Laboratory for their efforts that resulted in making NEAR Shoemaker the first spacecraft to orbit and land on an asteroid. The NEAR-Shoemaker mission and this work were made possible by NASA. We thank A. Rivkin and M. Cintala for suggestions.

Correspondence and requests for materials should be addressed to M.S.R. (e-mail: robinson@earth.northwestern.edu).

# Experimental long-lived entanglement of two macroscopic objects

**Brian Julsgaard, Alexander Kozhekin & Eugene S. Polzik**

*Institute of Physics and Astronomy, University of Aarhus, 8000 Aarhus, Denmark*

**Entanglement is considered to be one of the most profound features of quantum mechanics[1,2]. An entangled state of a system consisting of two subsystems cannot be described as a product of the quantum states of the two subsystems[3–6]. In this sense, the entangled system is considered inseparable and non-local. It is generally believed that entanglement is usually manifest in systems consisting of a small number of microscopic particles. Here we demonstrate experimentally the entanglement of two macroscopic objects, each consisting of a caesium gas sample containing about $10^{12}$ atoms. Entanglement is generated via interaction of the samples with a pulse of light, which performs a non-local Bell measurement on the collective spins of the samples[7]. The entangled spin-state can be maintained for 0.5 milliseconds. Besides being of fundamental interest, we expect the robust and long-lived entanglement of material objects demonstrated here to be useful in quantum information processing, including teleportation[8–10] of quantum states of matter and quantum memory.**

In 1935 Einstein, Podolsky and Rosen (EPR) formulated[1] what they perceived as a paradox created by quantum mechanics. Since then, the EPR correlations and other types of entanglement have been extensively analysed, notably by Bell[2]. Entangled or inseparable states are fundamental to the field of quantum information, specifically to quantum teleportation of discrete[8,9] and continuous[10] variables and to quantum dense coding of discrete[11] and continuous[12,13] variables, to name a few examples. The majority of experiments on entanglement until now deal with entangled states of light[3,4,8–11,14]. Entangled states of discrete photonic variables (spin-half systems)[3,4] as well as entangled states of continuous variables (quadrature-phase operators) of the electro-magnetic field[14] have been generated experimentally. Entangled states of material particles are much more difficult to generate experimentally; however, such states are vital for storage and processing of quantum information. Recently, entangled states of four trapped ions have been produced[15], and two atoms have been entangled via interaction with a microwave photon field[16].

Here we describe an experiment on the generation of entanglement between two separate samples of atoms containing $10^{12}$ atoms each, along the lines of a recent proposal[7]. Not only do we demonstrate a quantum entanglement at the level of macroscopic objects, our experiment proves feasible a new approach to the quantum interface between light and atoms suggested in refs 7, 17. It is a step towards the other protocols proposed[7,17], such as the teleportation of atomic states and quantum memory. The entanglement is generated through a non-local Bell measurement on the two samples' spins, performed by transmitting a pulse of light through the sample.

The ideal EPR entangled state of two sub-systems described by continuous non-commuting variables $\hat{X}_{1,2}$ and $\hat{P}_{1,2}$—such as the positions and momenta of two particles, for example—is the state for which $\hat{X}_1 + \hat{X}_2 \to 0$, $\hat{P}_1 - \hat{P}_2 \to 0$. Recently[5,6], the necessary and sufficient condition for the entanglement or inseparability for such gaussian quantum variables has been cast in the form of an inequality involving only the variances of variables: $\langle(\delta(\hat{X}_1 + \hat{X}_2))^2\rangle + \langle(\delta(\hat{P}_1 - \hat{P}_2))^2\rangle < 2$. In our experiment, the quantum variables that are analogous to the position and momentum operators are two projections of the collective spin (total angular momentum) of an atomic sample. The analogy is evident from the commutation relation $[\hat{J}_x, \hat{J}_y] = i\hat{J}_z$, which can be rewritten as $[\hat{X}, \hat{P}] = i$, where $\hat{X} = \hat{J}_y/\sqrt{J_x}$ and $\hat{P} = \hat{J}_z/\sqrt{J_x}$ if the atomic sample is spin-polarized along the $x$ axis with $\hat{J}_x$ having a large classical value $J_x$. For two spin-polarized atomic samples with $J_{x1} = -J_{x2} = J_x$, the above entanglement condition translates into

$$\delta J^2_{y12} = \delta J^2_{y12} + \delta J^2_{y12} < 2J_x \qquad (1)$$

where we introduce the notations $\delta J^2_{z12} = \langle(\delta(\hat{J}_{z1} + \hat{J}_{z2}))^2\rangle$ and $\delta J^2_{y12} = \langle(\delta(\hat{J}_{y1} + \hat{J}_{y2}))^2\rangle$. The interpretation of condition (1) comes from the recognition of the fact that for both atomic samples in coherent spin states (CSS) the equality $\delta J^2_{z,z} = J_x/2$ holds, that is, the inequality (1) becomes the equality. Entanglement between atoms of the two samples is, therefore, according to condition (1), equivalent to spin variances that are smaller than in samples in a CSS[18,19] characterized by uncorrelated individual atoms. The entangled state of this type is a two-mode 'squeezed' state for the continuous spin variables[5,7]. A spin squeezed state of a single macroscopic atomic ensemble has been generated previously[21,22].

Entanglement is produced via interaction of atoms with polarized light. A polarized pulse of light is described by Stokes operators obeying the same commutation relation as spin operators $[\hat{S}_x, \hat{S}_y] = i\hat{S}_z$. $\hat{S}_x$ is the difference between photon numbers in $x$ and $y$ linear polarizations, $\hat{S}_y$ is the difference between polarizations at $\pm 45^\circ$, and $\hat{S}_z$ is the difference between the left- and right-hand circular polarizations along the propagation direction, $z$. In our experiment light is linearly polarized along the $x$ axis. Hence the two pairs of continuous quantum variables engaged in the entanglement protocol are $\hat{J}_z$ and $\hat{J}_y$ for atoms and $\hat{S}_z$ and $\hat{S}_y$ for light.

Here we report on the generation of a state of two separate caesium gas samples (Fig. 1), which obey the entanglement condition (1). As shown in refs 7 and 17, when an off-resonant pulse is transmitted through two atomic samples with opposite mean spins $J_{x1} = -J_{x2} = J_x$, the light and atomic variables evolve as

$$\begin{aligned} &\hat{S}_y^{out} = \hat{S}_y^{in} + \alpha\hat{J}_{z12}, \hat{S}_z^{out} = \hat{S}_z^{in} \\ &\hat{J}_{y1}^{out} = \hat{J}_{y1}^{in} + \beta\hat{S}_z^{in}, \hat{J}_{y2}^{out} = \hat{J}_{y2}^{in} - \beta\hat{S}_z^{in}, \hat{J}_{z1}^{out} = \hat{J}_{z1}^{in}, \hat{J}_{z2}^{out} = \hat{J}_{z2}^{in} \end{aligned} \qquad (2)$$

where $\alpha$ and $\beta$ are constants. The first line describes the Faraday effect (polarization rotation of the probe). The second line shows the back action of light on atoms, that is, spin rotation due to the angular momentum of light. According to equations (2), the measurement of $\hat{S}_y^{out}$ reveals the value of $\hat{J}_{z12} = \hat{J}_{z1} + \hat{J}_{z2}$ (provided $\alpha$ is large enough, so that $\hat{S}_y^{in}$ is relatively small) without changing this value. It follows from equations (2) that the total $y$ spin projection for both samples is also conserved, $\hat{J}_{y1}^{out} + \hat{J}_{y2}^{out} = \hat{J}_{y1}^{in} + \hat{J}_{y2}^{in}$. The procedure can be repeated with another pulse of

  

light measuring the sum of $y$ components, $\hat{J}_{y1} + \hat{J}_{y2}$, again in a non-demolition way, while at the same time leaving the previously measured value of $\hat{J}_{z1} + \hat{J}_{z2}$ intact. As a result, the sum of the $z$ components and the sum of the $y$ components of the spins of the two samples are known exactly in the ideal case, and therefore the two samples are entangled according to condition (1), since the uncertainties on the left-hand side become negligible.

An important modification of the above protocol is the addition of a magnetic field oriented along the direction $x$, which allows us to use a single entangling pulse to measure both $z$ and $y$ spin projections, as described in the Methods section.

The schematic of the experimental set-up is shown in Fig. 1. The two cells are coated from inside with a paraffin coating which enhances the ground-state coherence time $T_2$ up to 5–30 ms depending on the density of atoms. $|J_x|$ and $T_2$ are measured by the magneto-optical resonance method (ref. 20 and references therein).

After the samples are prepared in CSS, as described in the legend to Fig. 1, optical pumping is switched off and a probe pulse is sent through. Its Stokes operator $S_y$ is measured by a polarizing beam splitter with two balanced detectors. The differential photocurrent from the detectors is split in two and its $\cos(\Omega t)$ and $\sin(\Omega t)$ power spectral components $(S^{\text{out}}_{y\cos}(\Omega))^2$ and $(S^{\text{out}}_{y\sin}(\Omega))^2$ are measured by lock-in amplifiers. By repeating this sequence many times we obtain the variances for these components, in short, spectral variances, which according to equation (3) in the Methods section are $(\delta S^{\text{out}}_{y\cos}(\Omega))^2 = (\delta S^{\text{in}}_{y\cos}(\Omega))^2 + 1/2\alpha^2\delta\hat{J}^2_{z12} = 1/2\delta S^2 + \kappa\delta\hat{J}^2_{z12}$, where $\kappa = \frac{1}{2}\alpha^2$, and similarly for $(\delta S^{\text{out}}_{y\sin}(\Omega))^2$ with substitution $J_z \to J_y$. The coefficient $\alpha = \sigma\gamma n/4FA\Delta \approx 2.5$ is estimated[17] using $\sigma = \lambda^2/2\pi$ as the resonant dipole cross-section, $\gamma = 5$ MHz as the full width of the optical transition, $F = 4$ as total angular momentum of the hyperfine ground state, $A = 2\,\text{cm}^2$ as the probe beam cross-section, and $n = 10^{12}$ as the number of photons in the 0.45 ms probe pulse with power 5 mW.

The spectral variance data, $\Delta = (\delta S^{\text{out}}_{y\cos}(\Omega))^2 + (\delta S^{\text{out}}_{y\sin}(\Omega))^2 = \delta S^2 + \kappa\delta\hat{J}^2_{z12} + \kappa\delta\hat{J}^2_{y12} \approx \delta S^2 + \kappa\delta\hat{J}^2_{y}$, is plotted in Fig. 2. The linear fit to it, $\Delta(J_x)$, is the quantum limit of noise corresponding to the coherent spin state of samples (see Fig. 2 legend for details).

Using $\Delta(J_x)$ as a reference level we can now devise a measurement procedure, which will verify the presence of an entangled state. Namely, if for a certain state of the two ensembles the spectral variance of the signal $\Delta_{\text{EPR}} = \delta S^2 + \kappa\delta\hat{J}^2_{\text{EPR}}$ obeys the inequality:

$$\Delta_{\text{EPR}} = \delta S^2 + \kappa\delta\hat{J}^2_{\text{EPR}} < \delta S^2 + 2\kappa J_x = \Delta(J_x) \qquad (4)$$

then apparently $\delta\hat{J}^2_{\text{EPR}} < 2J_x$ holds for such a state and therefore this state is entangled in accordance with condition (1). It is, of course, necessary to use otherwise identical conditions for measurements of $\Delta_{\text{EPR}}$ and $\Delta(J_x)$, that is, the same value of $2J_x$ and the same probe intensity and detuning in order to keep the constant $\kappa$ unchanged throughout the entire experiment. As mentioned above, the value of $2J_x$ has been controlled by a magneto-optical resonance measurement to better than 5%. In the actual experiment described below the measurements of $\Delta_{\text{EPR}}$ and $\Delta(J_x)$ have been conducted in turn at identical conditions at the repetition rate of 500 Hz.

The measurement sequence aimed at the generation and verification of the entanglement consists of the optical pumping pulses, which induces a CSS, the entangling pulse, which induces an entangled state (pulse I) in the samples, and the verifying pulse, which occurs after a delay time $\tau$ and verifies the entanglement (pulse II). These pulses have the same duration and optical frequency as the probe pulse used for the CSS measurements. Between the two pulses the joint spin state of the two samples is subject to decoherence. The photocurrents from the two pulses are subtracted electronically and the variance of the difference, $\Delta_{\text{EPR}}$, is

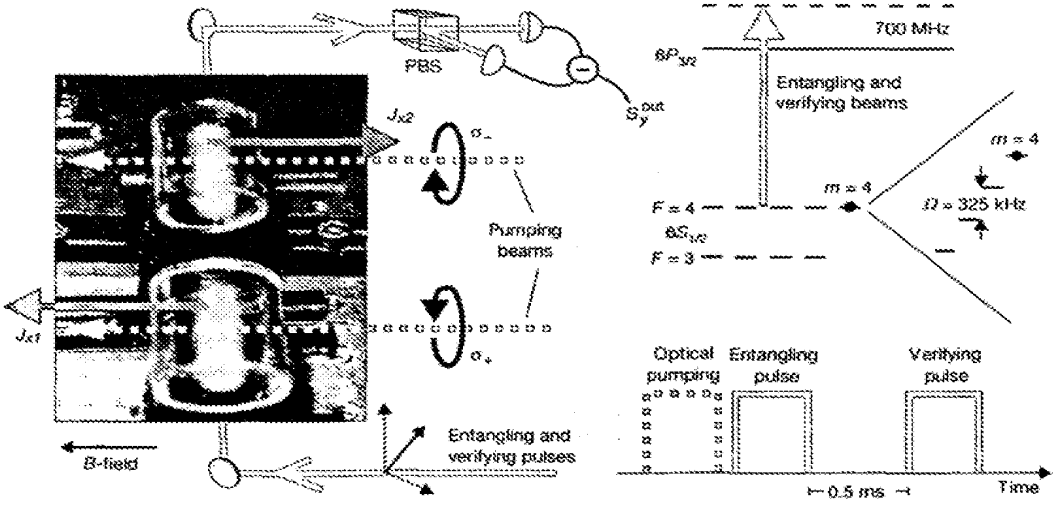


**Figure 1** The experimental set-up, atomic level structure and the sequence of optical pulses. Fluorescence of atoms interacting with light is seen inside the cells (artificial colour). The two atomic samples in glass cells 3 × 3 cm at approximately room temperature are placed in a highly homogeneous magnetic field of 0.9 G ($\Omega = 325$ kHz) surrounded by a magnetic shield. Caesium atoms are optically pumped into $F = 4$, $m_F = 4$ ground state in the first cell and into $F = 4$, $m_F = -4$ in the second cell to form coherent spin states oriented along the $x$ axis for cell 1 and along $-x$ for cell 2. Optical pumping is achieved with circularly polarized 0.45 ms pulses at 852 nm and 894 nm with opposite helicity for the two cells. The mean spin value for each sample is given by $J_x = N\sum_{m=-4}^{4} m p_m \approx 4Np \to 4N$, where $N$ is the number of atoms and $p_m$ is the probability of an atom being in the $m$ state, with the limiting value corresponding to a perfect spin polarization, $p = 1$. The $|J_x|$ for the two cells is adjusted to be equal to or better than 5%. After the optical pumping is completed 0.45 ms long entangling and verifying pulses separated by a 0.5-ms delay are sent through. Both pulses are blue-detuned by $\Delta = 700$ MHz from the closest hyperfine component of the $D_2$ line at 852 nm. The thermal atomic motion is not an obstacle in this experiment but is rather helpful. The probe beam covers most but not the whole volume of the atomic sample, but the duration of the pulses is longer than the transient time of an atom across the cell. Therefore each light pulse effectively interacts with and entangles all atoms of the samples. In addition, a large detuning of the probe makes the Doppler broadening insignificant.

measured as discussed in the Methods section. The vanishing $\Delta_{EPR}$ corresponds to two repeated measurements on the total spin state of the two samples producing the same results, that is, it corresponds to a perfect knowledge of both $\hat{J}_{z12}$ and $\hat{J}_{p12}$ and therefore to a perfectly entangled state. In the experiment the minimal value of $\Delta_{EPR}$ is $2\delta S^2$ owing to the quantum noise of the entangling and verifying pulses.

The results of measurements with $\tau = 0.5$ ms are shown in Fig. 3. The results are normalized to the CSS limit $\Delta(J_x)$ (the linear fit in Fig. 2). This limit thus corresponds to the unity level in Fig. 3. The raw experimental data $\Delta_{EPR}/\Delta(J_x)$ for the entangled state are shown as stars. The values below the unity level verify that the entangled state of the two atomic samples has been generated and maintained for 0.5 ms. The derivation of the degree of entanglement from the data in Fig. 3 is given in the Methods section. The degree of entanglement calculated operationally from the data without additional assumptions is $\xi = (35 \pm 7)\%$. The degree of entanglement useful for teleportation that was calculated using an additional, experimentally proved assumption of the initially CSS for both samples is higher, $\xi' = (52 \pm 7)\%$. The predicted teleportation fidelity performed with the same two pulses as used in the present paper (see Methods section) is $\mathcal{F} = 55\%$, which is above the classical limit of 50%. The factors limiting the fidelity are of a technical nature, and we expect higher fidelity to be well within reach.

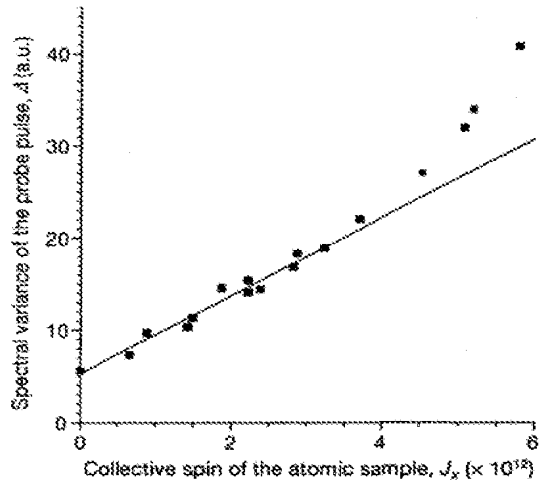


**Figure 2** Determination of the coherent spin state limit for entanglement. The total measured variance of the two quadratures of the photocurrent $\Delta = (\delta S^{out}_{max}(\Omega))^2 + (\delta S^{out}_{min}(\Omega))^2 = \delta S^2 + \kappa\delta J^2_{z12} + \kappa\delta J^2_{p12} = \delta S^2 + \kappa\delta J^2_{12}$ is plotted as a function of $J_x$. $J_x$ is measured independently by magneto-optical resonance method and is varied by heating the cells and by adjusting optical pumping. In the absence of atoms in the cells the measured spectral variance is due to the initial probe state variance $\delta S^2$. $\delta S^2$ is at the vacuum (shot) noise level, which has been verified experimentally by checking its characteristic linear dependence on the probe power. With atoms present the measured variance grows linearly with $J_x$ at low densities, which proves that there is no classical contribution to the spin noise and that therefore the observed atomic fluctuations at these densities are entirely due to quantum atomic noise[21]. The degree of the spin polarization for the data in the figure (shown as squares) is nearly perfect, $p \geq 95\%$, which means that the spin state is very close to the coherent spin state (CSS). We therefore conclude that a linear fit to the observed data corresponds to the CSS of both atomic samples for which $\delta J^2_{12} = 2J_x$ and hence this line, which we denoted by $\Delta(J_x)$, establishes the noise level corresponding to the right-hand side of the inequality (4). Deviations of the observed variance from the linear fit at high atomic numbers are due to the nonlinearly growing contribution of classical technical noise of the spin state because of the technical noise of lasers, the non-ideal cancellation of the back action of the probe on the two samples, and so on.

The imperfect entanglement comes from several factors. First, the vacuum noise of the entangling pulse prohibits a perfect preparation of the spin state, especially for a small number of atoms. Second, the deviation of the initial spin state from CSS, which is due to the classical noise of the lasers, becomes more pronounced as the number of atoms grows. Finally, losses of light on the way from one cell to another, as well as the spin-state decay between the two measurements preclude perfect entanglement at all atomic densities. The spin-state decay is caused by collisions and the quadratic Zeeman effect.

Measurements with delay times longer than 0.8 ms demonstrate no entanglement. The decoherence process can be illustrated by visualizing two ellipses in the phase space, corresponding to the two samples, with the size along the long axes of the order of three, in units of the coherent state (experimentally measured value). When the ellipses start to dephase (rotate) the total noise along the short axis becomes equal to the coherent state noise (zero degree of entanglement) after the time of the order of 1.2 ms if the initial entanglement of 65% (maximal degree allowed by the experimental light noise) is assumed. After a 0.6-ms delay a degree of entanglement of 35% should be expected, given the experimentally measured dephasing time of 5 ms. These numbers agree reasonably well with observations.

It is instructive to analyse the difference between the degree of entanglement and the degree of classical correlations. For uncorrelated atomic samples the normalized variance of the difference between the two photocurrents would be equal to two, using the notation of Fig. 3. The pure atomic part of this variance $V_{uncorr}$ would be approximately 1.5 for medium atomic densities. For the actual data in Fig. 3 the atomic part of the variance is approximately $V_{corr} = 0.25$. The degree of correlation, $1 - V_{corr}/V_{uncorr}$, is 83% for this example. This number is much higher than the degree of

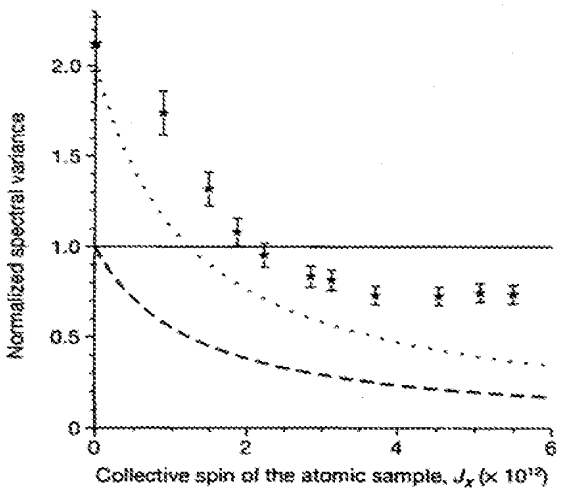


**Figure 3** Demonstration of the entangled spin state for two atomic samples. The results are plotted as a function of $J_x$ and are normalized to the CSS limit $\Delta(J_x)$ (the linear fit in Fig. 2). This limit—the boundary between entangled (below the line) and separable states—thus corresponds to the unity level in the figure (solid line). The raw experimental data $\Delta_{EPR}/\Delta(J_x)$—data for the entangled spin state, which has lived for $\tau = 0.5$ ms—are shown as stars. The values below the unity level verify that the entangled state of the two atomic samples has been generated and maintained for 0.5 ms. The minimal possible level for $\Delta_{EPR}/\Delta(J_x)$ (maximum possible entanglement) is equal to $2\delta S^2/\Delta(J_x)$ (dotted line), that is, it is set by the total quantum noise of the two pulses. The normalized shot noise level of the verifying pulse, $\delta S^2/\Delta(J_x)$ (dashed line), which is used for calculations of the degree of entanglement, is also shown.

entanglement, implying that entanglement requires something stronger than classical correlations. The reason for this difference is that in quantum mechanics the measuring device (light in this case) becomes entangled with the measured object and therefore the noise of these two subsystems cannot be treated independently.

Thus, we have demonstrated on-demand generation of entanglement of two separate macroscopic objects, which can be maintained for more than 0.5 ms. The state we have demonstrated is not a maximally entangled 'Schrödinger's cat' state, which for $10^{12}$ atoms would not survive even for a femtosecond under the conditions of our experiment. Our state is similar to a two-mode squeezed state, and is an example of a non-maximally entangled state which is suitable for a particular purpose, for example, atomic teleportation. The long lifetime of this multi-particle entanglement is due to a high symmetry of the generated state. Entanglement manifests itself only in the collective properties of the two ensembles. Therefore a loss of coherence for a single atom makes a negligible effect on the entanglement, unlike in a maximally entangled multi-particle state. The entanglement is generated by means of light propagating through the two samples and therefore the samples can be distant, as is required for communications. The off-resonant character of the interaction used for the creation of entanglement allows for the potential extension of this method to other media, possibly including solid-state samples with long-lived spin states. □

## Methods

### Entangling spin components with a single light pulse

The Larmor precession of the $J_x, J_y$ components with a common frequency $\Omega$ does not change their mutual orientation and size and therefore does not affect the entanglement. On the other hand, the precession allows us to extract information about both $x$ and $y$ components from a single probe pulse as described below. Moreover, in the laboratory frame the spin state is now encoded at the frequency $\Omega$, and as usual an a.c. measurement is easier to reduce to the quantum noise level than a d.c. measurement. Measurements of the light noise can now be conducted only around its $\Omega$ spectral component. By choosing a suitable radio-frequency value for $\Omega$ we can reduce the probe noise $\delta S^{\text{in}}_{y,z}(\Omega)$ to the minimal level of the vacuum (shot) noise. In the presence of the magnetic field the spin behaviour is described by the following equations: $\dot{J}_x(t) = \Omega J_z(t), \dot{J}_z(t) = -\Omega J_x(t) + \beta S_y(t)$, whereas the Stokes operators still evolve according to equation (2). Solving the spin equations and using equation (2) we obtain

$$S_y^{\text{out}}(t) = S_y^{\text{in}}(t) + \alpha\{J_{x0}\cos(\Omega t) + J_{z0}\sin(\Omega t)\} \tag{3}$$

The $J_{x,y}$ components are now defined in the frame rotating with the frequency $\Omega$ around the magnetic field direction $x$. It is clear from equation (3) that by measuring the $\cos(\Omega t)/\sin(\Omega t)$ component of $S_y^{\text{out}}(t)$ we can acquire the knowledge of the $z/y$ spin projections. Simultaneous measurement of both spin components of the two atomic samples is possible because they commute: $[J_{1x} + J_{2x}, J_{1y} + J_{2y}] = i(J_{1z} + J_{2z}) = 0$.

### Degree of entanglement

The differential noise for the entangling (pulse I) and verifying (pulse II) pulses can be expressed using equation (3) as:

$$\begin{aligned}\Delta_{\text{ERR}} &= \delta S^2_{\text{out}} + \delta S^2_{\text{in}} \propto (\delta S^{\text{slow}}_{y\text{out}}(\Omega) - \delta S^{\text{slow}}_{y\text{out}}(\Omega))^2 + (\delta S^{\text{slow}}_{y\text{out}}(\Omega) - \delta S^{\text{slow}}_{y\text{in}}(\Omega))^2 \\ &\propto \delta S^2_{\text{in}} + \alpha^2\left\{\kappa^{-1}\delta S^2_{\text{in}} + [\delta(J_{x1\tau} - \delta(J_{y1})_0]^2 + [\delta(J_{z1\tau} - \delta(J_{z1})_0]^2\right\} \\ &\propto \delta S^2_{\text{in}} + \alpha\delta J^2_{\text{ERR}}\end{aligned} \tag{5}$$

The variance $\delta J^2_{\text{ERR}}$ determines the uncertainty of the spin components of the state prepared by the entangling pulse and measured after time $\tau$. It contains two contributions: $\delta S^2_{\text{in}}$, due to the quantum noise of the entangling pulse, and all other terms in the curly brackets, which are due to decoherence during the time $\tau$. The verifying pulse in our experiment is also not noiseless and therefore its variance, $\delta S^2_{\text{in}}$, also contributes to $\Delta_{\text{ERR}}$. In the experiment $\delta S^2_{\text{in}} = \delta S^2_{\text{in}} = \delta S^2$. The exact entanglement condition, $\Delta_{\text{ERR}} < \Delta(J_x)_0$ is obtained by substituting equation (5) into equation (4). The degree of entanglement can be defined as $\xi = 1 - (\delta J^2_{\text{ERR}}/2J_x) = 1 - (\Delta_{\text{ERR}} - \delta S^2)/(\Delta(J_x) - \delta S^2)$. $\xi$ varies from 0 (separable state) to 1 (perfect entanglement). The highest degree of entanglement calculated operationally from the data is $\xi \approx (35 \pm 7)\%$.

An alternative calculation of the degree of entanglement can be carried out[7], which takes into account that the initial state of both samples is characterized by the CSS noise level. Equation (2) of ref. 7, using the notation of the present paper, yields for the highest possible degree of entanglement (defined again as $\xi = 1 - (\delta J^2_{\text{ERR}}/2J_x)$) and created by the *first* pulse *in our protocol*, the value $\xi_{\text{theory}} = 1 - \eta_{\text{theory}}$ where the degree of the "two-mode squeezing" is, according to ref. 7, $\eta_{\text{theory}} = \delta S^2/(\delta S^2 + 2\kappa J_x) = \delta S^2/\Delta(J_x)$. This is *the best entanglement possible for a given ratio of the light noise and the atomic spin noise contribution*. This value of entanglement would correspond to the minimal possible difference between the two pulses, $\Delta^{\text{min}}_{\text{ERR}} = 2\delta S^2$. We note that this value is closer to unity (stronger entanglement) than the degree of entanglement $\xi = 1 - (\Delta^{\text{min}}_{\text{ERR}} - \delta S^2)/(\Delta(J_x) - \delta S^2) = 1 - \delta S^2/(\Delta(J_x) - \delta S^2)$ calculated in the previous paragraph. This is because the entanglement in ref. 7 is calculated assuming that the samples prior to entanglement are known to be in the CSS. This fact has been experimentally verified in the present paper for up to intermediate atomic densities, so we may use this way of calculating the degree of entanglement at these densities as well. However, we are interested in the degree of entanglement, which has survived the delay time and which has been measured by the verifying pulse. For various reasons, including the decoherence *during the delay time*, the *differential noise between the two pulses does not reduce* to its minimal value, $\Delta_{\text{ERR}} > \Delta^{\text{min}}_{\text{ERR}} = 2\delta S^2$. Therefore the actual degree of entanglement, as witnessed by the measurement, is lower than the maximum possible: $\xi' = 1 - \eta_{\text{expt}} < \xi_{\text{theory}}$. Here the degree of squeezing, $\eta_{\text{expt}} = (\Delta_{\text{ERR}} - \delta S^2)/\Delta(J_x) > \eta_{\text{theory}}$ obtained from the data in Fig. 3 is worse than the theoretical best value, $\eta_{\text{theory}}$, owing in part to the diffusion of the state during the delay time between the entangling and the verifying pulses. From Fig. 3 we find $\eta_{\text{expt}} = 0.48$ and therefore $\xi' = 52\%$ for $J_x = 3.5 \times 10^{12}$.

### Expected fidelity of teleportation

It is also possible to estimate the fidelity of teleportation which would be achieved if the second, verifying pulse were (instead of verification) used for the Bell measurement on one of the entangled samples and a sample to-be-teleported. Using the value of $\xi'$ and equation (3) from ref. 7 we obtain a value for the fidelity of teleportation of $\mathcal{F} = 55\%$ for $J_x = 3.5 \times 10^{12}$. This is higher than the classical boundary of $\mathcal{F} = 50\%$.

We note that the entangled state reported here has a random element in it, namely, every (ideal) entangling measurement creates the state $J_{x1} + J_{x2} = x, J_{y1} + J_{y2} = p$ with $x, p$ random measured values. However, this state is as efficient for teleportation, for example, as a state $J_{x1} + J_{x2} = 0, J_{y1} + J_{y2} = 0$.

Received 11 June; accepted 27 July 2001.


1. Einstein, A., Podolsky, B. & Rosen, N. Can quantum-mechanical description of physical reality be considered complete? *Phys. Rev.* **47**, 777–780 (1935).
2. Bell, J. S. *Speakable and Unspeakable in Quantum Mechanics* (Cambridge Univ. Press, Cambridge, 1988).
3. Aspect, A., Dalibard, J. & Roger, G. Experimental test of Bell's inequalities using time-varying analyzers. *Phys. Rev. Lett.* **49**, 1804–1807 (1982).
4. Tegerson, J. R., Branning, D., Monken, C. H. & Mandel, L. Experimental demonstration of the violation of local realism without Bell inequalities. *Phys. Lett. A* **204**, 323–328 (1995).
5. Duan, Lu. M., Giedke, G., Cirac, J. I. & Zoller, P. Inseparability criterion for continuous variable systems. *Phys. Rev. Lett.* **84**, 2722–2725 (2000).
6. Simon, R. Peres-Horodecki separability criterion for continuous variable systems. *Phys. Rev. Lett.* **84**, 2726–2729 (2000).
7. Duan, L. M., Cirac, J. I., Zoller, P. & Polzik, E. S. *Phys. Rev. Lett.* **85**, 3645–3648 (2000).
8. Bouwmeester, D., Pan, J. W., Mattle, K., Eibl, M., Weinfurter, H. & Zeilinger, A. Experimental quantum teleportation. *Nature* **390**, 575–579 (1997).
9. Boschi, D., Branca, S., De Martini, F., Hardy, L. & Popescu, S. Experimental realization of teleporting an unknown pure quantum state via dual classical and Einstein-Podolsky-Rosen channels. *Phys. Rev. Lett.* **80**, 1121–1125 (1998).
10. Furusawa, A. *et al.* Unconditional quantum teleportation. *Science* **282**, 706–709 (1998).
11. Mattle, K., Weinfurter, H., Kwiat, P. G. & Zeilinger, A. Dense coding in experimental quantum communication. *Phys. Rev. Lett.* **76**, 4656–4659 (1996).
12. Braunstein, S. L. & Kimble, H. J. Dense coding for continuous variables. *Phys. Rev. A* **61**, 042302 (2000).
13. Ban, M. Quantum dense coding via a two-mode squeezed-vacuum state. *J. Opt. B* **1**, L9–L11 (1999).
14. Ou, Z. Y., Pereira, S. F., Kimble, H. J. & Peng, K. C. Realization of the Einstein-Podolsky-Rosen paradox for continuous variables. *Phys. Rev. Lett.* **68**, 3663–3666 (1992).
15. Eckert, C. A. *et al.* Experimental entanglement of four particles. *Nature* **404**, 256–259 (2000).
16. Rauschenbeutel, A. *et al.* Step-by-step engineered multiparticle entanglement. *Science* **288**, 2024–2028 (2000).
17. Kuzmich, A. & Polzik, E. S. Atomic quantum state teleportation and swapping. *Phys. Rev. Lett.* **85**, 5639–5642 (2000).
18. Kitagawa, M. & Ueda, M. Spin squeezed states. *Phys. Rev. A* **47**, 5138–5143 (1993).
19. Wineland, D. J., Bollinger, J. J., Itano, W. M., Moore, F. L. & Jeomtzen, D. J. Spin squeezing and reduced quantum noise in spectroscopy. *Phys. Rev. A* **46**, R6797–R6800 (1992).
20. Kopeiyanov, D. V. & Sokolov, I. M. Optical detection of magnetic resonance by classical and squeezed light. *Quant. Opt.* **4**, 55–70 (1992).
21. Hald, J., Sorensen, J. L., Schori, C. & Polzik, E. S. Spin squeezed atoms: a macroscopic entangled ensemble created by light. *Phys. Rev. Lett.* **83**, 1319–1322 (1999).
22. Kuzmich, A., Mandel, L. & Bigelow, N. P. Generation of spin squeezing via continuous quantum nondemolition measurement. *Phys. Rev. Lett.* **85**, 1594–1597 (2000).



### Acknowledgements

We gratefully acknowledge the contributions of J. Hald, J. L. Sørensen, C. Schori and A. Verchovski. We also thank I. Cirac, A. Kuzmich, A. Sørensen and P. Zoller for discussions.


Correspondence and requests for materials should be addressed to E.P. (e-mail: polzik@ifa.au.dk).